

Nanometric deformations of thin Nb layers under a strong electric field using soft x-ray laser interferometry

G. Jamelot, D. Ros, A. Carillon, B. Rus, T. Mocek et al.

Citation: *J. Appl. Phys.* **98**, 044308 (2005); doi: 10.1063/1.2010620

View online: <http://dx.doi.org/10.1063/1.2010620>

View Table of Contents: <http://jap.aip.org/resource/1/JAPIAU/v98/i4>

Published by the [American Institute of Physics](#).

Additional information on *J. Appl. Phys.*

Journal Homepage: <http://jap.aip.org/>

Journal Information: http://jap.aip.org/about/about_the_journal

Top downloads: http://jap.aip.org/features/most_downloaded

Information for Authors: <http://jap.aip.org/authors>

ADVERTISEMENT



**FIND THE NEEDLE IN THE
HIRING HAYSTACK**

Post jobs and reach
thousands of hard-to-find
scientists with specific skills



<http://careers.physicstoday.org/post.cfm> **physicstoday JOBS**

Nanometric deformations of thin Nb layers under a strong electric field using soft x-ray laser interferometry

G. Jamelot,^{a)} D. Ros, and A. Carillon

Laboratoire d'Interaction du rayonnement X Avec la Matière, Unité Mixte de Recherche (UMR) n° 8624, Université Paris-Sud and Centre National de la Recherche Scientifique (CNRS), Bâtiment 350, 91405 Orsay, France

B. Rus, T. Mocek, M. Kozlová, and A. R. Präg

Department of X-ray Lasers, Institute of Physics/Prague Astrix Laser System (PALS) Research Centre, 18221 Prague 8, Czech Republic

D. Joyeux and D. Phalippou

Laboratoire Charles Fabry de l'Institut d'Optique, Bâtiment 503, 91403 Orsay, France

M. Boussoukaya, M. Kalmykow, F. Ballester, and E. Jacques

Service d'Etude des Accélérateurs, Commissariat à l'Energie Atomique, Centre d'Etudes Nucléaires de Saclay, 91191 Gif sur Yvette, France

(Received 28 February 2005; accepted 11 July 2005; published online 18 August 2005)

We present measurements of *in situ* nanometric-resolution topographical modifications of thin niobium layers subjected to strong electric fields. The Nb layers, deposited on a fused silica substrate, are interferometrically flash probed using soft x-ray laser (XRL) at the wavelength of 21.2 nm. Its pulses are reflected by the probed sample under grazing incidence angle, and the information about surface deformation is obtained by a Fresnel wave-front-division interferometer. It was experimentally established that the probing pulses at the soft x-ray wavelength do neither produce any measurable photoelectric-field emission, nor alter the topographical features of the probed surface. The examined Nb electrodes were periodically probed while the electric field was increased up to 80 MV/m, and alterations of their topographical characteristics with a resolution of ~ 2 nm in the relief elevation were obtained. It was found that behavior of the Nb layer strongly depends on the polarity of the applied voltage. Only small modifications are observed with the Nb surface at the positive potential, whereas the negative potential induces significant transient surface perturbations, with peak-to-valley elevation differences ~ 50 nm. The qualitative nature of these modifications was observed to be unrelated to intermittent parasitic breakdowns. © 2005 American Institute of Physics. [DOI: 10.1063/1.2010620]

I. INTRODUCTION

Metallic surfaces submitted to intense electric fields emit electrons.^{1,2} While significant field emission, resulting in appreciable current for cathodes of approximately cm^2 size, is theoretically expected to occur typically at electric fields to the order of GV/m, large emission currents are experimentally detected at much lower-field strengths. This field emission limits the attainable value of the applied electric field, which is a serious limitation for building superconducting linear accelerators and colliders (such as teraelectron volt energy superconducting linear accelerator (TESLA), with a goal to produce beam energy of 1 TeV), namely, of its injecting devices based on rf cavities.³ The field-emitted electrons impact on the cavity surface, leading to its heating and consequently increasing its electrical resistance. In an extreme case, field emission of the cavity walls can lead to thermal breakdown. The field emission and the below-threshold breakdowns phenomena limit rf electric fields in the present experimental superconducting structures to values between 15 and 20 MV/m and lead to significant additional costs to reach the projected parameters.

To understand the detrimental effects of field emission, it is imperative to determine to which extent the dissipative phenomena are related to the nature of the sample, or whether they originate in external elements due to the fabrication process.⁴

Scanning electron microscopy⁵ and scanning tunneling microscopy⁶ have shown links between field emission and surface contaminants and/or minute surface defects. However, these diagnostics provide information about the surface only after its exposure to the electric field is terminated (the rf cavity is cut apart to allow examination), hence do not allow visualization during the field emission, or accessing surface alterations ahead of the breakdown. High-resolution *in situ* thermometry, using an array of temperature sensors, has been used to provide the heat patterns due to impacting electrons originated from a field emitter, e.g., in rf niobium cavity at 1.6 K.⁷ While it is possible with this technique to localize some field-emission sites, the field emitters exhibit rather complex morphology, and no information is provided about the surface before the electrons are emitted.

Interferometry using soft x-ray laser pulses offers qualitatively an alternative technique of *in situ* surface mapping, able to distinguish nanometric altitude features at the same

^{a)}Electronic mail: gerard.jamelot@lixam.u-psud.fr

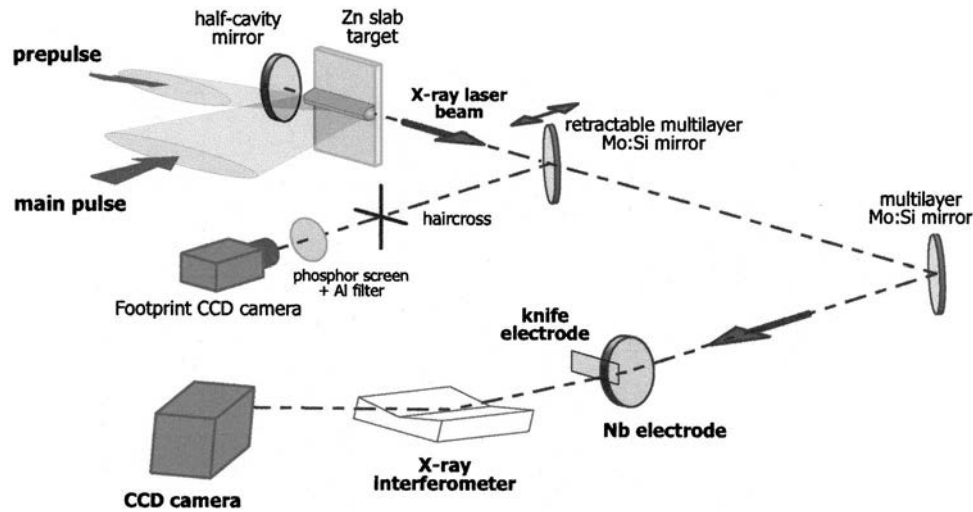


FIG. 1. Experimental arrangement of the soft x-ray laser and the interferometric arm (not to scale). The XRL beam is switched between the footprint monitor and the interferometer by a retractable multilayer mirror working at 45° . Another multilayer mirror at 45° sends the beam to the interferometer, polarizing it vertically.

time as the electron emission occurs. It was demonstrated in our earlier work,⁸ in which it was applied to visualization of modifications of a surface of bulk niobium, subjected to electric field. In addition to nanometer altitude resolution capability due to the wavelength, a major advantage of soft x-ray and interferometry is that the probing electromagnetic wave totally reflects off a metallic surface when incident at small grazing angle, since the real part of the refraction index ($n = 1 - \delta - i\beta$) for x rays is less than 1. In contrast with the case of visible or UV light, the frequency of the incident soft x-ray wave is higher than the plasma frequency of a metal, and the mechanisms of reflection qualitatively differ as a result. Due to the comparably low optical frequency, the visible or UV light, incident on a metallic surface under a strong electric bias field, will likely affect the electron field emission. The optical wave induces on the metal a resonant surface current, which, in conjunction with the associated large magnetic field of the penetrating damped wave,⁹ is capable to produce field enhancement on microscopic imperfections of the surface (see, e.g., Ref. 4). This problem is dramatically reduced for soft x rays with its frequency above the metal plasma frequency, since the amplitudes of the induced surface current and of the associated magnetic field are much smaller.

On the other hand, the critical angle of niobium, at the wavelength of 21.2 nm of the soft x-ray laser employed, is $\theta_c = 37.5^\circ$ (measured up from the surface). A beam incident at a grazing angle of 6° will produce evanescent wave with a penetration depth of only 2.7 nm.¹⁰ Also, in this experiment, the probing soft x-ray beam is *s* polarized when incident on the Nb cathode, which further decreases the penetration depth inside the investigated surface.

The XUV interferometry of nonstationary surfaces requires monochromatic-pulsed sources of high brightness. Synchrotron radiation is therefore not suitable, since it calls for rather long exposure times. In contrast, x-ray lasers provide an ideal radiation source due to their short pulse (<100 ps), delivered in a narrowly collimated and highly

coherent beam. This makes it possible to probe the examined surface in a snapshot and to visualize, with nanometric altitude resolution, transient surface alterations inaccessible by other techniques.

In this paper we present results of investigation of the behavior of thin Nb layers deposited on fused silica substrates, subjected to fields up to 80 MV/m, with both positive and negative polarities.

II. EXPERIMENTAL SETUP

The experiment was performed at the PALS (Prague Asterix Laser System) facility,¹¹ using its iodine IR laser to pump a plasma-based soft x-ray laser emitting at the wavelength of 21.2 nm. A schematic view of the experimental arrangement is shown in Fig. 1. The x-ray laser is generated on the surface of a zinc slab, by a pump sequence consisting of a weak (~ 2 J) prepulse, followed after 10 ns by the main pulse delivering ~ 500 J of net energy. The x-ray laser (XRL) beam emerging from the amplifying plasma may be detected either as a “footprint” via a flat retractable Mo:Si multilayer mirror or sent by another multilayer mirror towards the x-ray interferometer, reflecting on its path off the probed Nb surface. The multilayer mirrors operate at an incidence angle of 45° and besides acting as a cut-off filter for keV x-ray and UV emissions, they work as soft x-ray polarizers, since 45° incidence angle approximately corresponds to the Brewster’s angle.¹² The reflected XRL beam is consequently *s* polarized (electric vector parallel to the polarizer).

A. X-ray laser

The soft x-ray laser operated at PALS (Ref. 13) provides strongly amplified emission at 21.2 nm, corresponding to the $J=0-1$ transition $(2p_{1/2}^5 3p_{1/2})_{J=0} \rightarrow (2p_{1/2}^5 3s_{1/2})_{J=0}$ in neon-like zinc. It operates in double-pass regime, employing a 3-cm-long plasma and flat half-cavity Mo:Si multilayer mirror located 8.5 mm from the plasma end. The prepulse and the main pumping pulse have both duration of ~ 400 ps and gen-

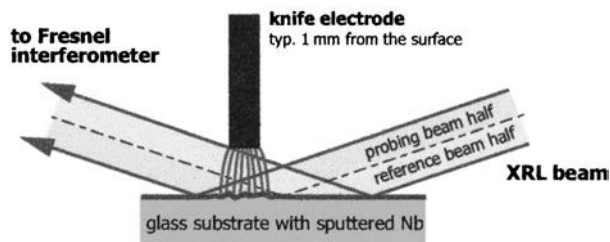


FIG. 2. Schematic of the niobium-coated flat substrate and an iron knife electrode system, showing the principle of the probing technique (not to scale).

erate x-ray lasing action in the “quasistationary state” (QSS) regime, which is characteristic by a high output energy but requires relatively large pump device. Here, the deeply saturated double-pass XRL beam provides ~ 4 mJ of energy in ≈ 80 -ps pulses, corresponding to a peak power in excess of 40 MW. The x-ray laser shot at the PALS facility may be fired every 20 min.

The amplifying plasma column is generated in a regime in which the main pulse, producing net target irradiance of $\sim 2.8 \times 10^{13} \text{ Wcm}^{-2}$, is focused significantly more tightly ($\sim 130 \mu\text{m}$) than the prepulse ($\sim 700 \mu\text{m}$). In conjunction with the half cavity and a uniform main pulse focus generated by a composite lens matrix,¹⁴ this arrangement produces an XRL beam exhibiting a high spatial quality as well as excellent shot-to-shot reproducibility; the respective horizontal and vertical divergences of the beam are ~ 4 and ~ 6 mrad.

B. Niobium electrodes and electrical circuit

The Nb electrodes used in this work were deposited by ion-beam magnetron sputtering on 15-mm-diameter super-polished, fused silica substrates with rms surface roughness of $\sim 15 \text{ \AA}$. The thickness of the Nb layer is about $0.5 \mu\text{m}$. The working potential of such a layer is approximately equal to 4.3 eV that of bulk Nb. The samples were kept under neutral atmosphere (N_2) until the moment of their installation into the vacuum chamber. The experiment was performed under vacuum of about 10^{-6} Torr at room temperature.

The second electrode was constituted by a thin iron knife (see Fig. 1), 10 mm large and $600 \mu\text{m}$ thick. Its distance from the Nb surface, which was typically 1 mm, as well as its parallelism with this surface, was carefully adjusted.

Figure 2 shows the geometry under which the Nb layers were probed by the XRL beam. The beam is incident on the surface under a grazing angle of 6° , which is significantly smaller than the critical angle of 37.5° for the 21.2-nm radiation, and makes the niobium about 90% reflective for s polarization at this wavelength. As mentioned earlier, the evanescent wave associated with the reflected XRL beam and penetrating into the layer is very weak.

As seen from Fig. 2, the knife-edge electrode is placed asymmetrically with respect to the substrate center, about 3.5 mm to one side. Thus the first half of the XRL beam provides, upon reflection off the unperturbed Nb surface, the

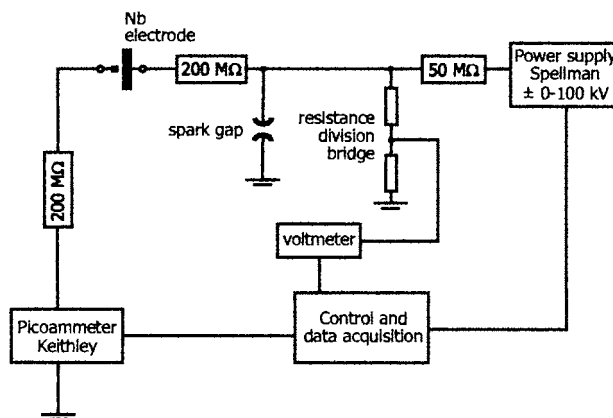


FIG. 3. Setup of the HV electric circuit. Both positive and negative voltages up to 100 kV may be applied to the system Nb electrode-knife edge.

reference wave front, whereas the second half of the beam carries information about the deformed surface underneath the knife electrode.

The setup of the employed high-voltage (HV) electrical circuit is shown in Fig. 3. The circuit produces dc electric field with amplitudes on the Nb surface from 0 to 100 MV/m. The electric current passing by the sample is measured each 300 ms by a picoammeter which integrates the charge over 80 ps. A spark gap protects the picoammeter against high electric currents due to possible breakup and breakdown. The measurements were made with both polarities. In the first case, the Nb layer was at the negative potential and acted as electron emitter. In the second case, the Nb layer was at the positive potential and acted as electron collector.

C. X-ray interferometer

The device employed to analyze the wave front of the x-ray beam reflected off the probed Nb surface is a Fresnel bimirror interferometer.^{15,16} It belongs to the class of wave-front-division interferometers and constitutes a versatile tool utilizable over a wide spectral range in the x-ray and XUV domain. Due to its robustness and simple alignment, it may be easily employed in conjunction with an x-ray laser,¹⁷ constituting an alternative to amplitude-division devices.^{18,19} Compared to the other prototype of wave-front-division interferometer, namely, the Lloyd mirror,²⁰ the Fresnel bimirror presents two decisive advantages. First, the separation of any pair of interfering rays is constant across the field, thus avoiding fringe modulations from spatial coherence issues. Second, the fringe spacing is independent of the beam incidence onto the bimirror, while in the Lloyd case, incidence must be kept highly grazing, which makes fringe adjustment much more tricky.

The geometry of the interferometer and a scheme of its implementation in the experiment are shown in Fig. 4. The interferometer consists of a tandem of adjacent high-quality plane mirrors $15 \times 60 \text{ mm}^2$, inclined to each other at a small angle (5.2 mrad) and fixed on a common support. The x-ray beam reflected off the Nb cathode is incident on the tandem of mirrors in the plane of symmetry of the system, containing the line along which the mirrors join. Upon reflection, the

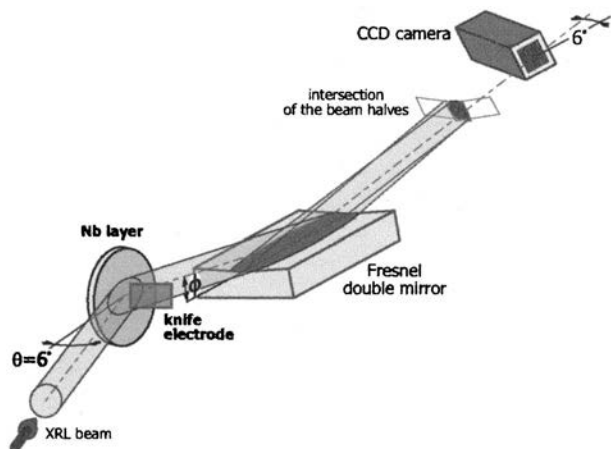


FIG. 4. Fresnel bimirror interferometer, analyzing the x-ray beam reflected from the vertically orientated Nb cathode (not to scale); the probing XRL beam is vertically polarized. The cathode is located at a distance of ~ 300 cm from the XRL exit aperture and a few centimeters before the Fresnel bimirror; the optical distance between the bimirror and the CCD camera is 70 cm. The grazing incidence of the CCD is 6° in order to enhance the apparent fringe shift.

beam is split up vertically, with respect to the plane of incidence, into two halves. The beam halves propagate with a small angle toward each other and produce interference pattern as they overlap. It may be easily shown that for a parallel beam, the fringe period equals $\lambda/(2\phi\varepsilon)$, where ϕ is the grazing angle of incidence of the beam on the system (measured with respect to the central groove, see Fig. 4) and ε is the angle between the two mirrors. For a divergent XRL beam, emitted from a nearly point source, the fringe period is increased to $(\lambda/2\phi\varepsilon)D_2/D_1$, where D_2 and D_1 are, respectively, the optical distances of the detector and of the Fresnel bimirror from the source. For $\lambda=21.2$ nm, $\phi=6^\circ$, $\varepsilon=5.2$ mrad, $D_1=300$ cm, and $D_2=370$ cm, the fringe period is ~ 24 μm .

The resulting interferograms were detected by a phosphor-coated 512×512 pixel 12-bit charge-coupled device (CCD) camera (ARP Photonetique) with an active surface of 10×10 mm², located 70 cm downstream from the Fresnel bimirror. The camera was inclined to view the fringes under an angle of 6° (see Fig. 4), which is identical to that under which the x-ray laser beam probes the Nb electrode. The reason for this arrangement is twofold. First, it allows augmenting the detected fringe spacing by nearly one order of magnitude ($1/\sin 6^\circ=9.57$) to ~ 230 μm . Secondly, the camera thus “views” dimensionally undistorted image of the probed surface scale, without asymmetrical longitudinal stretching.

In the interferometric records, the fringe position is related to the altitude profile of the Nb electrode in actual lateral scale. In other words, the altitude profile is encoded into the phase of the cosine of the fringe pattern. The perturbed region under the knife electrode extends approximately through the center of the fringe pattern, along vertical direction. Given the angle of incidence $\theta=6^\circ$ of the XRL beam to the Nb electrode, a shift of one fringe corresponds to the elevation on the Nb surface equal to $\lambda/(2 \sin \theta) \approx 100$ nm.

III. PROCESSING OF THE INTERFEROGRAMS

The detected fringe pattern carries in principle “complete” information about the probed Nb surface, i.e., about its minute relief features as well as about its reflectivity being a function of the local value of the complex index of refraction. It theoretically constitutes a reflection hologram of the surface, with a tilted offset reference wave (see, e.g., Ref. 21). However, the holographic information encoded in the recorded pattern is in reality severely degraded by a number of experimental constraints. These include the limited spatial resolution due to the phosphor grain, due to the fiber-optic taper transmitting the image to the CCD chip, and due to the pixel size (19×19 μm^2). Other limitations come from small shot-to-shot variations of the intensity profile of the x-ray laser beam and from presumably uneven intensity response of the phosphor over its surface. Accordingly, both high and very low spatial frequencies in the interferograms carry only little physical information and are not employable in the analysis. The processing technique employed is therefore based solely on detection of the frequency shift of the interference fringes, rather than on holographic reconstruction.

The recorded interferograms are digitally processed by usual Fourier techniques using the fast Fourier transform algorithm. In summary, as the surface elevation is coded into phase modulation of a carrier (the fringe pattern), a phase demodulation of that carrier must be performed. This is obtained in the spectral domain by frequency shifting one side band of the fringe pattern towards zero, then low-pass filtering the spectrum, and finally back Fourier transform to the space domain, to get the complex modulation function, amplitude, and phase. As usual, phase unwrapping is required when the phase excursion is larger than 2π . As it is well known, unwrapping becomes problematic when signal/noise ratio is not large enough, leading to unphysical phase maps. This is why the low-pass filtering step must be adjusted to the actual signal/noise ratio, so that the phase noise does not dominate over the signal. Finally, the phase map is converted straightforwardly into elevation map, through $2h \sin \theta/\lambda = \phi/2\pi$.

Since there is no imaging between the probed Nb plane and the detector, the spatial resolution (along the surface) provided by the resulting image is limited by diffraction. Also, the tilt of the object and the observation planes with respect to the direction of propagation results in asymmetry in resolution along the horizontal and the vertical direction. It may be seen easily that the horizontal resolution is reduced by a factor of $1/\sin 6^\circ=9.57$, with respect to the vertical resolution. This latter can be assessed by considering the characteristic period of fringes in the Fresnel diffraction pattern,²² equal to $\sqrt{\lambda D}$, where D is the propagation distance. In this approach, features in the normal object plane much smaller than $\sqrt{\lambda D}/2$ will be smeared by diffraction. With $D=700$ mm, $\sqrt{\lambda D}/2$ amounts to ~ 60 μm ; thus the resolution along the Nb surface is 60 μm vertically $\times 600$ μm horizontally, i.e., about $32(h) \times 3(v)$ pixels.

The altitude resolution is limited by the phase noise in the fringe pattern. Therefore, we consider as a reasonable estimation the sigma of the phase fluctuations in phase pro-

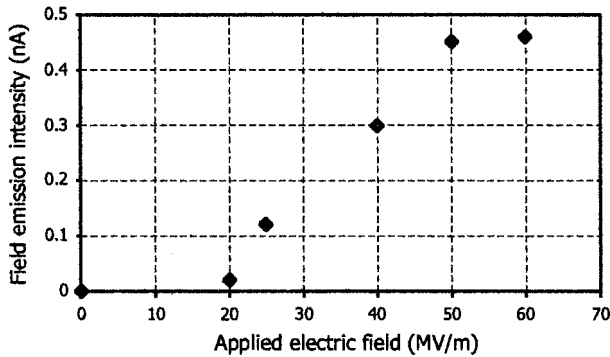


FIG. 5. Field-emission current measured at the negative polarity of the niobium cathode (Nb acts as an emitter of electrons), as a function of the applied dc voltage.

files obtained from interferograms without electrical field. As this is roughly equal to $2\pi/50$, and keeping in mind that one fringe shift corresponds to an altitude change of 100 nm (see Sec. II), the altitude resolution is about $100/50=2$ nm.

IV. EXPERIMENTAL RESULTS

In each of two series of the measurements, the first x-ray laser shot was carried out with zero voltage between the Nb layer and the knife electrode, in order to obtain the reference interferogram of unperturbed Nb surface. The electric field was then gradually increased by steps going along with the 20-min repetition rate of the x-ray laser; the field was maintained at a given value between two successive shots and was raised to the next-higher level shortly before firing the subsequent XRL shot. Two series of shots were taken with Nb layer at the negative potential, and one series with Nb at the positive potential.

A. Nb layer at the negative potential—electron emitter

In this configuration, the applied dc electric field was raised by steps from 0 to 60 MV/m. The measured average current passing through the electrode system, originating in the field emission, is displayed in Fig. 5. A measurable current—hence field emission—first appeared at 20 MV/m, amounting to 0.02 nA. This current increased to 0.46 nA while the applied field was risen 60 MV/m; these amplitudes imply that field emission of electrons from the Nb surface is rather fairly weak.

A sequence of x-ray interferograms recorded with the Nb layer at the negative dc potential up to 60 MV/m is shown in Fig. 6. It turns out that the individual records do not exhibit significant alteration of the fringe pattern with respect to the reference interferogram taken at zero field.

Figure 7 shows the reconstructed surface maps of the Nb layer, corresponding to the respective interferograms from Fig. 6. Up to 40 MV/m, only local surface elevations smaller than about 10 nm appear. At 50 MV/m, a horizontal ridge elevated by ~ 15 nm above the adjacent surface is detected; this ridge is not observed in the subsequent shot taken at 60 MV/m. We note that this feature, or other significant deviation from the plane surface, is not seen in the shots taken without electric field. This suggests that in this configuration the electric field produces small temporary elastic

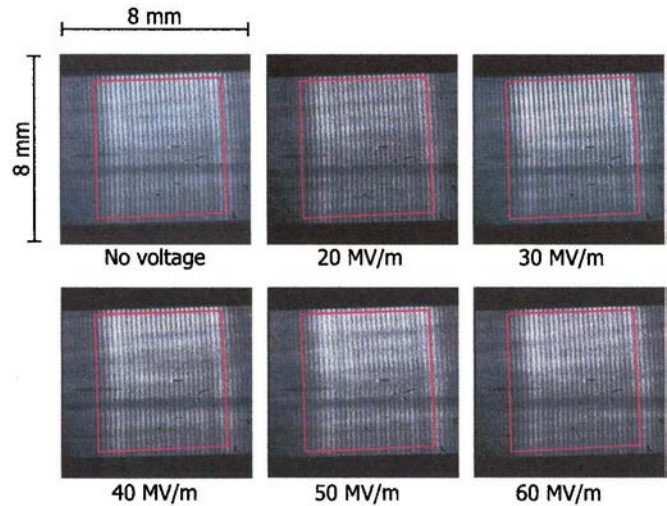


FIG. 6. (Color) A sequence of interferograms of the Nb surface at negative potential, subjected to dc field between 0 (reference) and 60 MV/m. The scale bar corresponds to the distance on the probed surface; fringe shift by one period corresponds to surface elevation of ~ 100 nm. The red quadrangles correspond to regions converted to the surface maps in Fig. 7.

deformations of the surface, which are apparently not connected to any permanent local characteristic of the Nb layer.

In the course of this probing sequence, an accidental microdischarge occurred about 10 min after the XRL shot taken at 30 MV/m, resulting in a short burst of the field-emission current of about $0.5 \mu\text{A}$. As seen from Fig. 7, this microbreakdown does, however, not result in any palpable modification of the Nb surface—no additional systematic surface feature emerges from the records taken at 40 MV/m and beyond.

B. Nb layer at the positive potential—electron collector

In this case, the applied dc electric field was gradually increased by steps from 0 to 72.5 MV/m. The measurement was carried out with a Nb layer identical to that used in a series with negative potential; the electrode remained uninterrupted in vacuum and was not subjected to any manipu-

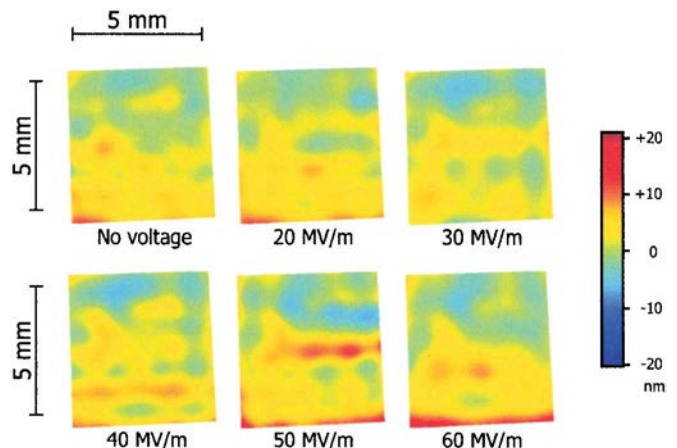


FIG. 7. (Color) Surface maps of the Nb layer at the individual values of the electric field, reconstructed from the corresponding interferograms shown in Fig. 6.

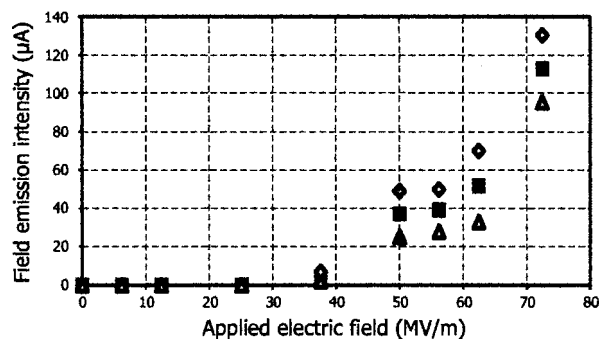


FIG. 8. Field-emission current with the Nb layer at positive potential (Nb acts as collector of electrons emitted from the knife electrode), accompanying the increasing bias voltage: ■=mean value of the current, △, ◇ =minimal and maximal values detected.

lation. Figure 8 shows the measured average current passing through the electrode system, where this time the Nb layer acts as collector of electrons emitted from the knife edge. Below 30 MV/m, the average current corresponding to field emission is low and stable, reaching approximately 80 pA at 25 MV/m. When the applied field is raised to 37.5 MV/m, the field-emission current increases to a significant value of about 2 μ A. Upon further increase to 50 MV/m, the field-emission electric current increased dramatically by more than one order of magnitude, reaching about 110 μ A at 72.5 MV/m. The current was observed to fluctuate significantly around a mean value, which is represented in Fig. 8 by its minimal and maximal values detected for each voltage; these fluctuations were seen to have characters of both slow variations and short-lived microflashings. It is worthy to note that no breakdown was seen to occur during this sequence.

The measured amplitudes of the electric current, contrasting with subnanoampere values when the Nb layer acted as an electron emitter, imply significant densities of current on the knife electrode, and consequently it heats up. This suggests that the field emission is in this case largely assisted by thermal effects. Furthermore, the large current amplitudes suggest that the thermal load of the Nb layer was significant in this configuration—the impacting electrons are accelerated by the electric field on their way towards the Nb surface.

Interferograms corresponding to the individual levels of the applied electric field are displayed in Fig. 9. While the interferogram taken at 37.5 MV/m reveals only moderate perturbation, above 50 MV/m the records exhibit large local fringe shifts and also intensity variations. These significant fringe perturbations are in stark contrast with the case with Nb at the negative potential. On the other hand, the difference between only a moderately perturbed interferogram at 37.5 MV/m and strong perturbations at 50 MV/m correlates well with the large enhancement of the field-emission current.

Figure 10 shows the topographical maps of the Nb surface, inferred from the respective interferograms in Fig. 9. At 37.5 MV/m, the field produces a localized apex near the center, elevated by \sim 20 nm above the neighboring slump. At 50 MV/m, the surface is strongly warped and exhibits nearly a continuous crest with peak-to-valley reaching \sim 40 nm; it is noteworthy that the crest direction does not simply follow

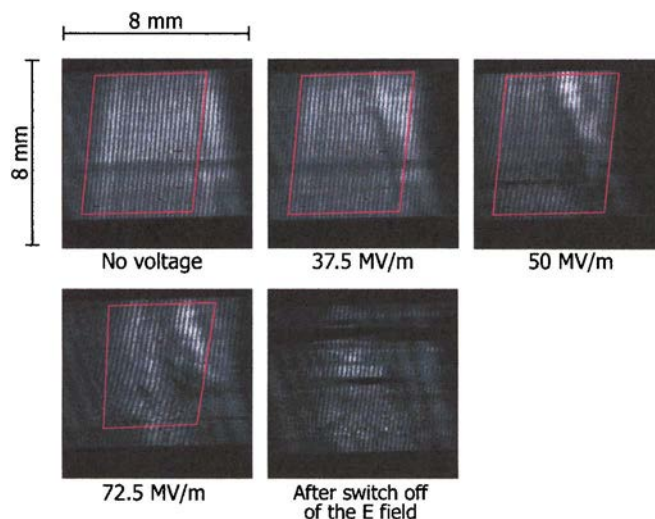


FIG. 9. (Color) A sequence of recorded interferograms for the niobium layer at positive potential, with electric field gradually increasing from 0 (reference) to 72.5 MV/m. The scale corresponds to the distance across the Nb surface; fringe shift by one period corresponds to surface elevation of about 100 nm. The red quadrangles correspond to regions converted to the surface maps in Fig. 10.

the vertical orientation of the knife electrode. At 72.5 MV/m, warp of the Nb layer extends further and the surface topography becomes further more complex, exhibiting local altitude differences of \sim 50 nm.

The last interferogram in Fig. 9 was taken about 26 min after the electric field (applied uninterruptedly over about 2 h) was turned off. The interferogram is not processed, because of large regions without interference fringes. These black streaks are an imprint of the Nb layer partially damaged or stripped away from the silica substrate and suggest that a major parasitic discharge occurred during the switch off of the electrical circuit. The fringes produced by the remaining surface are straight as in the initial interferogram, providing supplementary evidence that the surface warp observed throughout the sequence corresponds to actual transient deformations of the Nb surface, and that these deformations recede after the field is switched off.

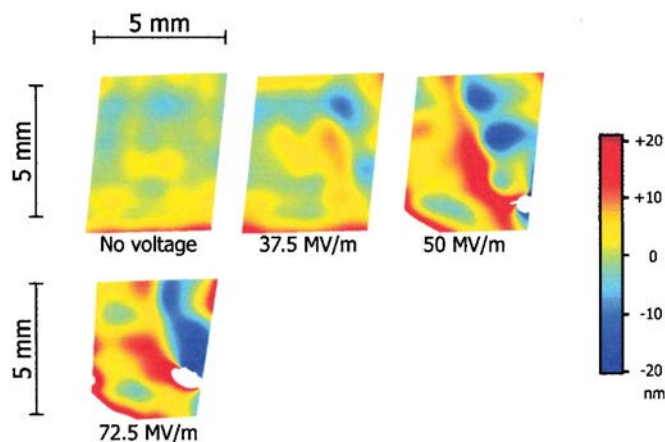


FIG. 10. (Color) Surface maps of the Nb layer at the individual values of the electric field, reconstructed from the corresponding interferograms from Fig. 9.

V. CONCLUSIONS

Soft x-ray laser interferometry at 21.2 nm was employed to visualize *in situ* deformations of thin niobium layers deposited on a silica substrate, subjected to dc electric fields up to 72.5 MV m^{-1} of both polarities. The topographical surface images obtained provide altitude resolution of $\sim 2 \text{ nm}$, the transverse resolution across the surface is $\sim 600 \times 60(h \times v) \mu\text{m}^2$. Along the interferometric probing, field-emission current between the examined Nb surfaces and the adjacent electrode was monitored throughout the entire experiment.

The current measurements affirm that the x-ray laser does not induce field emission from the probed surface, and that the detected values of field emission and the interferometric data reflect authentic behavior of the Nb layers under strong electric field. Besides, the images of a layer subjected consecutively to the same values of electric fields of opposite polarity, where identical electrostatic forces are involved, indicate that intrinsic local characteristics of the layer are not the principal factor involved in the observed deformations.

For both polarities, the series of interferometric images reveal that the deformations of the surface are principally elastic, as these disappear after the field is switched off. This behavior of thin niobium layers differs from that of slab Nb electrodes, which were observed to retain deformations more than 1 day after the switch off of the electric field.⁸

The magnitude of surface deformations is much larger when the Nb layer is electron collector than when it acts as electron emitter. The presumable reason is that in the former case the layer is locally heated by the impacting electrons, emitted from the opposite knife electrode. On the other hand, the data show that topography of the Nb surface warp is rather complex, and that the change of surface relief does not simply follow the geometry of the applied field. The likely explanation is that, at high values of the applied field, the spatial distribution of the electrons emitted from the knife electrode, which subsequently impact and heat the Nb layer, does largely depend on the local features of the knife electrode rather than on its macroscopic profile.

The interferometric data for the Nb surface acting as electron emitter show that intermittent thermal breakdowns and current thermoflashings do not significantly modify or damage the Nb surface—within both the lateral and the altitude resolution, no discernible changes of the surface topography are observed after the breakdown event. On the other hand, the strong surface modifications and local damage, seen when Nb is at positive potential, suggest that sites inducing geometric and/or thermal field enhancement are abundantly produced on such a perturbed surface. In the case of polarity-changing rf field, these sites would contribute to a substantial increase of the amplitude of field emission.

Finally, the measurements of the field-emission current reveal that for a given value of the applied field, thermal breakdown events occur at much lower rate than for slab Nb cathodes. When the Nb layer is at the negative potential, only a few breakdown and/or current thermoflashing events is encountered throughout the measurement sequence. At 60 MV/m , no thermal breakdown was detected, and the field-emission current remains at a fairly low level of 0.46 nA . This suggests that thin layers are possibly of high interest for accelerator applications, and that both surface deformations and basic photoelectron emission from, e.g., Nb, Cs_3Sb , or SiO_2 layers are worthy of further studies.

ACKNOWLEDGMENTS

We gratefully acknowledge the work of the PALS laser staff, as well as the design engineering of M. Hudecek and J. C. Lagron. We further thank P. Jaeglé, K. Jungwirth, K. Rohlena, J. Ullschmied, B. Aunc, and H. Safa for their support. This work financially benefited from the EU Transnational Access to Research Infrastructures Grant No. HPRI-00108, from the National Research Centres Project No. LN00A100 of the Ministry of Education of the Czech Republic, and from the Czech Academy of Sciences Grant No. A1010014.

¹R. H. Fowler and L. Nordheim, Proc. R. Soc. London, Ser. A **119**, 173 (1928).

²D. Moffat *et al.*, Part. Accel. **40**, 85 (1992).

³H. Padamsee, Supercond. Sci. Technol. **14**, R28 (2001).

⁴J. Knobloch, IEEE Trans. Appl. Supercond. **9**, 1016 (1999).

⁵J. Graber, J. Kirchgessner, D. Moffat, J. Knobloch, H. Padamsee, and D. Rubin, Nucl. Instrum. Methods Phys. Res. A **350**, 582 (1994).

⁶P. Niedermann and O. Fischer, IEEE Trans. Electr. Insul. **24**, 905 (1989).

⁷J. Knobloch and H. Padamsee, Part. Accel. **53**, 53 (1996).

⁸F. Albert *et al.*, Phys. Rev. B **60**, 11089 (1999).

⁹J. D. Jackson, *Classical Electrodynamics*, 2nd ed. (Wiley, New York, 1975).

¹⁰<http://www-cxro.lbl.gov>, Center for X-ray Optics, Lawrence Berkeley National Laboratory.

¹¹B. Rus, T. Mocek, A. R. Präg, J. C. Lagron, M. Hudecek, G. Jamelot, and K. Rohlena, J. Phys. IV **11**, Pr2-589 (2001).

¹²P. Dhez, Nucl. Instrum. Methods Phys. Res. A **261**, 71 (1987).

¹³B. Rus *et al.*, Phys. Rev. A **66**, 063806 (2002).

¹⁴B. Rus *et al.*, Plasma Phys. Controlled Fusion **44**, B207 (2002).

¹⁵J. Svatos, D. Joyeux, D. Phalippou, and F. Polack, Opt. Lett. **18**, 1367 (1993).

¹⁶F. Polack, D. Joyeux, J. Svatos, and D. Phalippou, Rev. Sci. Instrum. **66**, 2180 (1995).

¹⁷F. Albert *et al.*, Opt. Commun. **142**, 184 (1997).

¹⁸L. B. Da Silva *et al.*, Phys. Rev. Lett. **74**, 3991 (1995).

¹⁹J. L. A. Chilla, J. J. Rocca, O. E. Martinez, and M. C. Marconi, Opt. Lett. **21**, 955 (1996).

²⁰B. Rus *et al.*, in *X-Ray Lasers 2002*, edited by J. J. Rocca, J. Dunn, and S. Suckewer, AIP Conf. Proc. No. 641 (AIP, New York, 2002), p. 522.

²¹J. W. Goodman, *Introduction to Fourier Optics*, 2nd ed. (McGraw-Hill, New York, 1996).

²²E. Hecht, *Optics*, 4th ed. (Addison-Wesley, San Francisco, 2002).